Carbon nanotubes — chitosan nanobiocomposite for immunosensor

Ajeet Kaushik [a,b], Pratima R. Solanki [a], M.K. Pandey [a], Keiichi Kaneto [c], Sharif Ahmad [b], Bansi D. Malhotra [a,]

[a] Department of Science and Technology Centre on Biomolecular Electronics, National Physical Laboratory, New Delhi-110012, India
[b] Materials Research Laboratory, Department of Chemistry, Jamia Millia Islamia, New Delhi-110025, India
[c] Graduate School of Life Science and Systems Engineering, Kyushu Institute of Technology, Kitakyushu, 808-0196, Japan

ARTICLE INFO

Keyword:
Chitosan
CNTs
Carbon nanotubes
Nanobiocomposite
Immunosensor
Ochratoxin-A

ABSTRACT

Carboxylic group functionalized single walled (SW) and multi walled (MW) carbon nanotubes (CNT) have been incorporated into biopolymer matrix of chitosan (CH) to fabricate nanobiocomposite film onto indium–tin–oxide (ITO) coated glass plate for co-immobilization of rabbit-immunoglobulin (r-IgGs) and bovine serum albumin (BSA) to detect ochratoxin-A (OTA). The results of electrochemical studies reveal that presence of both CNT results in increased electro-active surface area of CH leading to enhanced electron transport in these nanobiocomposites. Moreover, in CH–SWCNT and CH–MWCNT nanobiocomposites the availability of NH_2/OH group in CH and surface charged CNT also increases loading of the r-IgGs resulting in enhanced electron transport responsible for improved sensing characteristics. Compared to BSA/r-IgGs/CH–MWCNT/ITO immunoelectrode, electrochemical response studies of BSA/r-IgGs/CH–SWCNT/ITO immunoelectrode carried out as a function of OTA concentration exhibits improved linearity as 0.25–6 ng/dL, detection limit as 0.25 ng/dL, response time as 25 s, and sensitivity as 21 μA ng dL^{-1} cm^{-2} with the regression coefficient as 0.998.

1. Introduction

Carbon nanotubes (CNT) due to their unique internal structure, electrical conductivity, high chemical activity, low mass density, high electro-active surface area, thermal stability and high mechanical strength have recently aroused much interest for the development of novel technological applications such as batteries, nano-electronic devices, fuel cells, as probe tips in scanning probe microscopy, supercapacitors, nano-transistors, electrochemical actuators, gas/bio sensors etc, [1,2]. Recently, surface-confined CNT due to their ability to promote electron transfer reactions with electro-active species have attracted much interest as potential candidates for the development of nanoscale electrochemical biosensors [3–12]. The structure-dependent metallic character of CNT should allow promotion of electron transfer reactions at low over potential. This characteristic along with the high surface area provides the favourable environment to immobilize desired biomolecules for unique biochemical sensing systems. The recent advances in increased production of well-controlled aligned carbon nanotube arrays have led to their application in biosensors technology [10].

CNT have been used as components in biological devices. However, the current focus is on attaching desired biomolecules onto CNT for biomedical applications.

It has been shown that small proteins can be entrapped into the inner channel of opened by adsorption via electrostatic interactions. The attachment of small proteins on the outer surface of CNT has been achieved, either by hydrophobic and electrostatic interactions via covalent bonding or by functionalization of the nanotube sides. CNT have the ability to accelerate electron transfer reactions involving different biomolecules such as dopamine [14], β-nicotinamide adenine dinucleotide (NADH) [15], norepinephrine [16], cytochrome c [17], ascorbic acid [18], 5-hydroxytrptamine [19], cysteine [20], homocysteine [21], nucleic acids [22] and cholesterol [12].

The aggregation of CNT due to their high surface free energy and existence of inter-tube vander Waals forces has limited their technological potential. The poor solubility of CNT in most solvents is a major barrier to development of CNT based nanodevices. Therefore, intrinsically hydrophobic surface of CNT can be functionalized covalently or non-covalently for obtaining increased biocompatibility, solubility and drug-loading capacity [12,13] for bio- medical applications.

These problems can perhaps be overcome by covalent attachment of CNT with alkyl chains and by non-covalent functionalization of CNT with conducting/bio polymers by preparing nanocomposites via hydrophobic or π–π interactions. The first approach disrupts the extended π-network at CNT surfaces resulting in their poor mechanical and electrical properties and the incorporation of CNT with polymeric backbone can be useful to improve solubility of CNT without changing their physical properties [12,13].

Conducting/bio polymer-CNT nanocomposites have been found to exhibit the properties of both the parent precursors along with its synergetic effect that is helpful for biosensor application [12,13,23–

25]. To optimize the use of CNT for bio-technological applications, it is necessary to functionalize CNT with biomaterials including biomolecules, biopolymers and other bio-nanostructures. Among the various biomaterials, chitosan (CH) a biopolymer is derived by the alkaline deacetylation of chitin found in the exoskeletons of shrimps and crabs. CH due to availability of amine/hydroxyl groups, non-toxicity, biocompatibility and excellent film can be used for wound dressings, carriers for drug delivery systems, artificial skin, space filling implants and most importantly to immobilize desired biomolecules for biosensor application [27]. In spite of these developments, there is a considerable scope to improve optical and electrical properties of CH via incorporation of CNT in the CH matrix to prepare nanobiocomposites for biosensing applications.

Zhang et al. [28] have fabricated CNT–CH platform for electrochemical sensing based on dehydrogenase enzymes. Luo et al. [25] have electrochemically deposited CH–MWCNT nanocomposite to obtain excellent electro catalytic ability in the reduction and oxidation of hydrogen peroxide (H_2O_2). Zhang et al. [26] have prepared electrochemical sensing platform based on the CNT/toluidine blue O–CH/CH system to facilitate electron transfer processes. DNA biosensors based on CH film doped with CNT has been prepared by Li et al. [29]. Liu et al. [30] have also studied direct electron transfer of glucose oxidase (GOx) in the CNT–CH nanocomposite matrix. Cui et al. [31] have prepared a novel CH/polyvinylimidazole–Os/CNT/lactate oxidase nanocomposite bioelectrode onto gold electrode for lactate detection. Wang et al. [32] have studied the fabrication of copper nanoparticle–CH–CNT/GCE for electrochemical sensing of H_2O_2 and glucose. Solanki et al. [33] have prepared nanobiocomposite film of MWCNT/CH–SiO_2 for the co-immobilization of cholesterol oxidase and cholesterol esterase to detect total cholesterol. Lin et al. [34] have prepared a sensitive amperometric immunosensor for α-fetoprotein in human serum based on CNT/gold nanoparticle/CH film onto GCE. In spite of these developments CH–CNT nanobiocomposite has not yet been explored for immunosensor application.

We report results of studies relating to the co-immobilization of r-IgGs and BSA onto COOH–CNTs and CH based nanobiocomposite films for ochratoxin-A (OTA) detection. OTA is the most abundant food contaminating mycotoxin found in tissues and organs of animals and human and is known to produce nephrotoxic, teratogenic, carcinogenic (Group 2B) and immune toxic activity in living beings, through consumption of improperly stored food products [35,36].

2. Experimental details

2.1. Materials

Chitosan (Mw 2.4×10^{-6}), ochratoxin-A (*Aspergillus ochraceus*), rabbit immunoglubin antibodies (r-IgGs), and bovine albumin serum (BSA; 98% purity) have been purchased from Sigma Aldrich. All these chemicals are of analytical grade and have been used without further purification. Indium–tin–oxide (ITO) coated glass plates have been obtained from Balzers, UK. The deionized water (resistance ~18 MΩ) from Millipore water purification system (Milli Q 10 TS) has been used for the preparation of the solutions and buffers.

2.2. Preparation of CH–SWCNTs/ITO and CH–MWCNTs/ITO nanobiocomposite electrode

Single walled carbon nanotubes (SWCNT) have been synthesized using the arc-discharge process using graphite/catalyst [nickel (8.6 wt.%), cobalt (8.6 wt.%)] composite electrode [37]. Multiwall carbon nanotubes (MWCNT) (90%) have been synthesized by catalytic chemical vapour deposition using a mixture of ferrocene and toluene as a source of catalyst and hydrocarbon, respectively [38]. These SWCNTs and MWCNT are then purified and functionalized (COOH group) and refluxed with concentrated boiling nitric acid for 12 h, and then washed with distilled water followed by rinsing with ethanol and drying at 60 °C [39].

The calculated amount of SWCNT (1 mg) and MWCNTs (1 mg) are dispersed in CH (0.50%) solution [prepared by dissolving CH (50 mg) in 100 mL of acetate buffer (0.05 M, pH 4.2)] by sonication for 12 h at room temperature (25 °C). The film of CH–SWCNT and CH–MWCNT nanobiocomposites are fabricated by dispersing 10 μL solution of both the nanobiocomposites onto an ITO (0.25 cm^2) surface allowing it to dry at room temperature for about 12 h in a controlled environment. These CH–SWCNT/ITO and CH–MWCNT/ITO nanobiocomposite films are washed with deionized water to remove unbound particles.

The electrochemical experiments using both CH–SWCNT/ITO and CH–MWCNT/ITO nanobiocomposite electrodes have been repeated in multiple sets and the results are reproducible within 1% variation indicating that both the nanobiocomposites are stable and can be used more than 25 times.

2.3. Immobilization of r-IgGs onto CH–SWCNT/ITO and CH–MWCNT/ITO nanobiocomposite electrode

OTA (*A. ochraceus*) solution is prepared in phosphate buffer (50 mM, pH 7.0) with 10% methanol. Solution of rabbit antibodies (r-IgGs) is prepared in phosphate buffer (50 mM, pH 7.0). Both the solutions containing 0.15 M NaN_3 as a preservative are aliquoated and stored at −20°C. The immobilization of r-IgG has been carried out by spreading 10 μL solution onto the CH–CNT electrode. Bovine serum albumin (BSA, 98 %) dissolved in phosphate buffer (50 mM, pH 7.0) is used as the blocking agent for non-specific binding sites.

2.4. Characterization

The FTIR spectra have been recorded on Perkin Elmer, Spectrum BX II spectrophotometer. Autolab Potentiostat/Galvanostat (Eco Chemie, Netherlands) is used for electrochemical studies such as cyclic voltammetry, differential pulse voltammetry and electrochemical impedance spectroscopy. These electrochemical measurements are carried out using a three-electrode cell with CH–SW/MWCNT/ITO nanobiocomposite electrode and BSA/r-IgGs/CH–SW/MW CNT/ITO immunoelectrode as the working electrode, platinum wire as the counter electrode, and saturated Ag/AgCl electrode as a reference electrode in phosphate buffer saline [PBS (50 mM, pH 7.0, 0.9% NaCl)] containing 5 mM $[Fe(CN)6]^{3-/4-}$.

3. Results and discussion

3.1. Fourier transform infrared spectroscopic studies

The functionalization of CNT, formation of CH–CNT nanobiocomposite and immobilization of r-IgGs and BSA onto CH–CNT nanobiocomposite films have been studied using Fourier transforms infrared (FTIR) spectroscopy (Fig. 1). IR spectra of SWNT (curve a, Fig. 1A) and MWCNT (curve b, Fig. 1A) exhibit bands that correspond to the functional groups of COOH–CNT. Both of the curves show peak at 1620 cm^{-1} due to the C–C graphitic stretching mode that is infrared-activated by extensive side-wall functionalization. The band at 1385 cm^{-1} is assigned to O–H deformation vibration mode due to adsorbed water, COOH group and partial oxidation of CNT, while in curve (b) the absorbance band at 1385 cm^{-1} is attributed to O–H deformation vibration of absorption water and –COOH, the band at 1100 cm^{-1} is assigned to the C–O stretching vibration. The weak band at 1740 cm^{-1} is attributed to the carbonyl stretching vibration in the –COOH groups reveals the COOH functionalization of CNT [39]. However, the IR bands in the spectra of SWCNT are well-resolved and are sharper than that of the MWCNT due to the open frame network of SWCNT resulting in improved electrical properties.

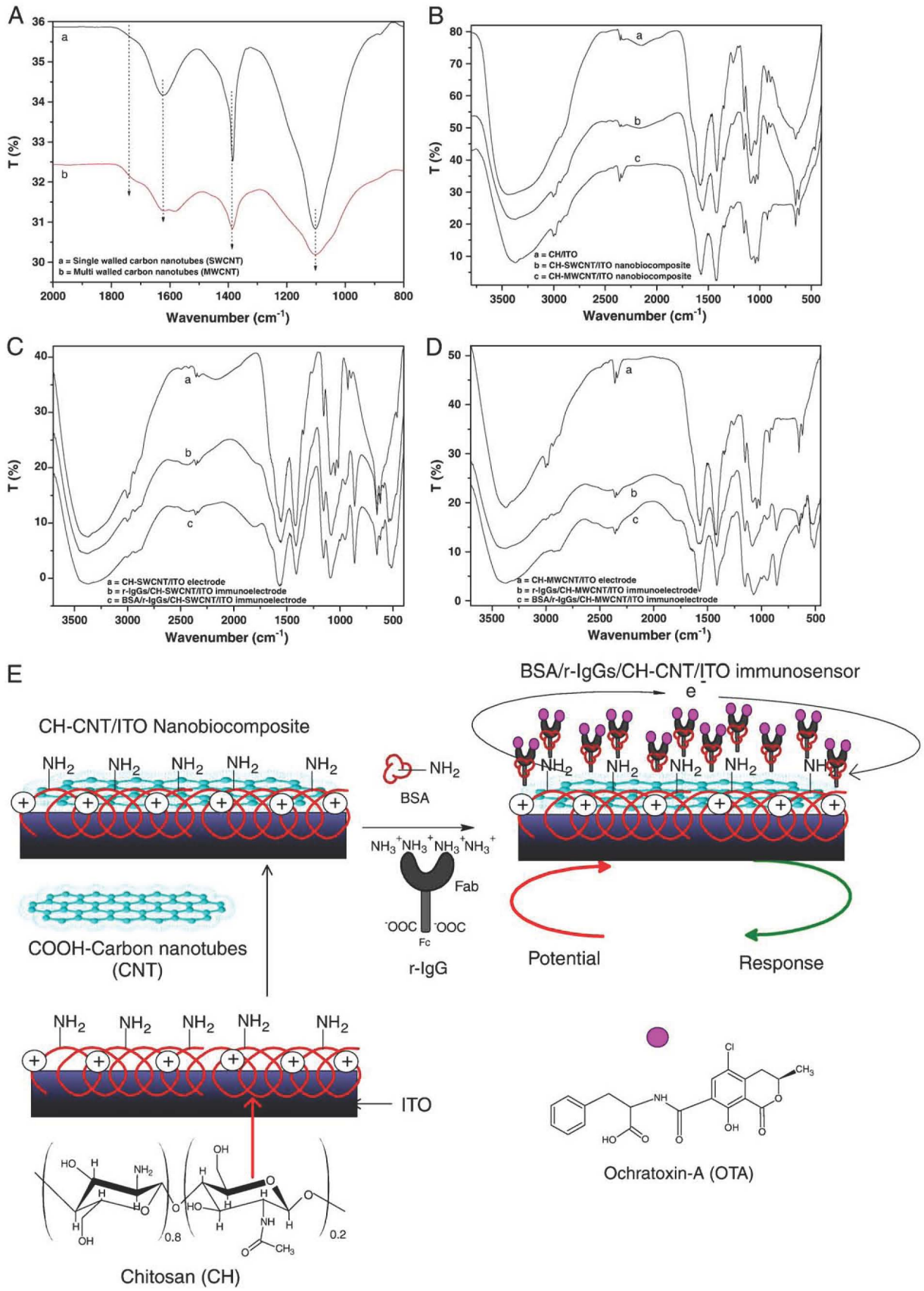

Fig. 1. FTIR spectra of A) SWCNT (curve a) and MWCNT (curve b). B) CH/ITO (curve a), CH–SWCNT/ITO nanobiocomposite (curve b) and CH–MWCNT/ITO nanobiocomposite electrodes (curve c). C) CH–SWCNT/ITO nanobiocomposite (curve a), r-IgGs/CH–SWCNT/ITO nanobiocomposite immunoelectrode (curve b) and BSA/r-IgGs/CH–SWCNT/ITO nanobiocomposite immunoelectrode (curve c). D) CH–MWCNT/ITO nanobiocomposite (curve a), r-IgGs/CH–MWCNT/ITO nanobiocomposite immunoelectrode (curve b) and BSA/r-IgGs/CH–MWCNT/ITO nanobiocomposite immunoelectrode (curve c). E) Proposed mechanism for the fabrication of BSA/r-IgGs/CH–CNT/ITO immunosensor and the biological reaction at the surface of the immunoelectrode.

FTIR spectra of CH (curve a, Fig. 1B) the IR band at bands at 3150–3500 cm^{-1} is due to the stretching vibration mode of OH and NH_2 group, 1650 cm^{-1} is due to the amide I group (C–O stretching along with N–H deformation mode), 1570 cm^{-1} peak is attributed to the NH_2 group due to N–H deformation, 1425 cm^{-1} peak is due to C–N axial deformation (amine group band), 1341 cm^{-1} peak is due to the COO^- group in carboxylic acid salt, 1150 cm^{-1} is assigned to the special broad peak of β (1–4) glucosidic band in polysaccharide unit, 1086 cm^{-1} is attributed to the stretching vibration mode of the hydroxyl group, 1020 cm^{-1} is due to the stretching vibration of C–O–C in the glucose circle. The band at 1060–1015 cm^{-1} is correspond to CH–OH in cyclic compounds. The IR corresponds to NH_2/OH group [40].

Fig. 1B shows the FTIR spectra of CH/ITO electrode (curve a), CH–SWCNT/ITO nanobiocomposite electrode (curve b) and CH–MWCNT/ITO nanobiocomposite electrode (curve c). The IR band of CH and SWCNT/MWCNT overlap in the spectrum of CH–SWCNT (curve b, Fig. 1B) and CH–SWCNT (curve c, Fig. 1B) nanobiocomposites respectively, because the functional group corresponds to CNTs and CH shows the IR bands in the same region. However, the shape and peak position of the band corresponds to the NH_2/OH groups of the CH changes in the spectra of CH–SWCNT and CH–MWCNT nanobiocomposite revealing the formation of nanobiocomposite due to the electrostatic interaction between CH and CNT. The IR band at 1080 cm^{-1} in the spectra of CH shifts toward the higher wavenumber 1090 cm^{-1} in the spectrum of both nanobiocomposites and reveals stretching vibration mode of hydroxyl groups in CH indicating interaction of CNT via hydrogen bonding. Moreover, the IR band at 1030 cm^{-1} in CH changes into a doublet at 1045 cm^{-1} and 1016 cm^{-1} in the spectrum of nanobiocomposites revealing that C–O–C group in glucose ring interact with CNT via weak interactions confirming the formation of CH–SWCNT and CH–MWCNT nanobiocomposites.

The FTIR spectra of r-IgGs and BSA immobilized CH–SWCNT/ITO and CH–MWCNT/ITO nanobiocomposite electrodes are shown in Fig. 1C and D. The presence of IR band at 1555 cm^{-1} observed in the spectra of r-IgGs/CH–SWCNT/ITO (curve b, Fig. 1C) and r-IgGs/ CH–MWCNT/ITO immunoelectrode (curve b, Fig. 1D) corresponds to amide II band of r-IgGs (β-sheet, main secondary structure element of IgG), indicating the presence of IgG immobilized onto the nanobiocomposite electrode. However, the presence on IR band at 1660 cm^{-1} and a sharp band 1572 cm^{-1} observed in the spectra of BSA/r-IgGs/CH–SWCNT/ITO (curve c, Fig. 1C) and BSA/r-IgGs/CH–MWCNT/ITO immunoelectrodes (curve c, Fig. 1D) corresponds to the amide II bands of BSA revealing the immobilization of BSA onto the r-IgGs/ nanobiocomposite electrode [42–43]. The new bands appearing at ~1053, ~955 and ~850 cm^{-1} in the spectra of r-IgGs and BSA and immobilized CH–SW/MWCNT/ITO electrodes are attributed to the N–H stretching mode in the amide group of proteins revealing the co-immobilization of r-IgGs and BSA onto CH–SWCNT/ITO and CH–MWCNT/ITO electrode.

The proposed mechanism of the fabrication of CH–SWCNT/ITO and CH–SWCNT/ITO nanobiocomposites, immobilization of r-IgGs and BSA onto both nanobiocomposites along with the biochemical reaction is shown in Fig. 1E. In our scheme, functionalized surface charged CNT interact with the cationic amine rich CH matrix via electrostatic interactions and hydrogen bonding (correlated by FTIR studies). To obtain an immunosensor of better sensing parameters, it is known that r-IgG molecules should be adsorbed in a favourable orientation wherein, the F_c (carboxyl terminated group) terminal of r-IgGs binds with nanobiocomposite electrode and its F_{ab} (amino terminated site) terminal should be free to bind with desired antigen. Both CH–SWCNT/ITO and CH–MWCNT/ITO nanobiocomposite electrodes bind with the carboxyl groups of r-IgG via electrostatic interactions and free amino terminal sites of r-IgG preferably bind with the carboxylic group of OTA molecules.

4. Electrochemical studies

Differential pulse voltammetry (DPV) studies of CH/ITO electrode (curve a), CH–MWCNT/ITO nanobiocomposite electrode (curve b) and CH–MWCNT/ITO nanobiocomposite electrode (curve c) are shown in Fig. 2A. It is clear that the CH/ITO electrode shows the well-defined reductive process due to the adsorption of redox [Fe(III)/Fe(IV)] probe onto the cationic CH/ITO electrode. The magnitude of the current response increases after the incorporation of CNT in CH matrix [CH–WMCNT (curve b) and CH–SWCNT nanobiocomposite (curve c)] revealing that the catalytic properties of CNTs increase the electractive surface area of CH resulting in improved electronic and ionic transport capacity of CH–CNT nanobiocomposite because CNT provides a three-dimensional electron conductive network extended throughout the ion-conductive matrix of CH. However, the magnitude of the electrochemical current response for CH–SWCNT/ITO nanobiocomposite electrode is higher than that of the CH–MWCNT/ITO nanobiocomposite electrode due to the high local density of electronic states in SWCNT, which has been attributed to their helicity and possible topological defects resulting in enhanced electron transfer kinetics in mediator at CH–SWCNT/ITO nanobiocomposite.

These results are further confirmed using electrochemical impedance spectroscopy (EIS, Fig. 2B). EIS is a powerful technique for studying the electrochemical properties of materials at the interface of the electronically conducting electrodes. The Nyquist plot of EIS spectra includes a semicircle portion at higher frequencies corresponding to the electron transfer limited process and a linear portion at lower frequencies corresponding to the diffusion process. The electron transfer resistance (R_{CT}) at the electrode surface is equal to the semicircle diameter, which can be used to describe the interface properties of the electrode.

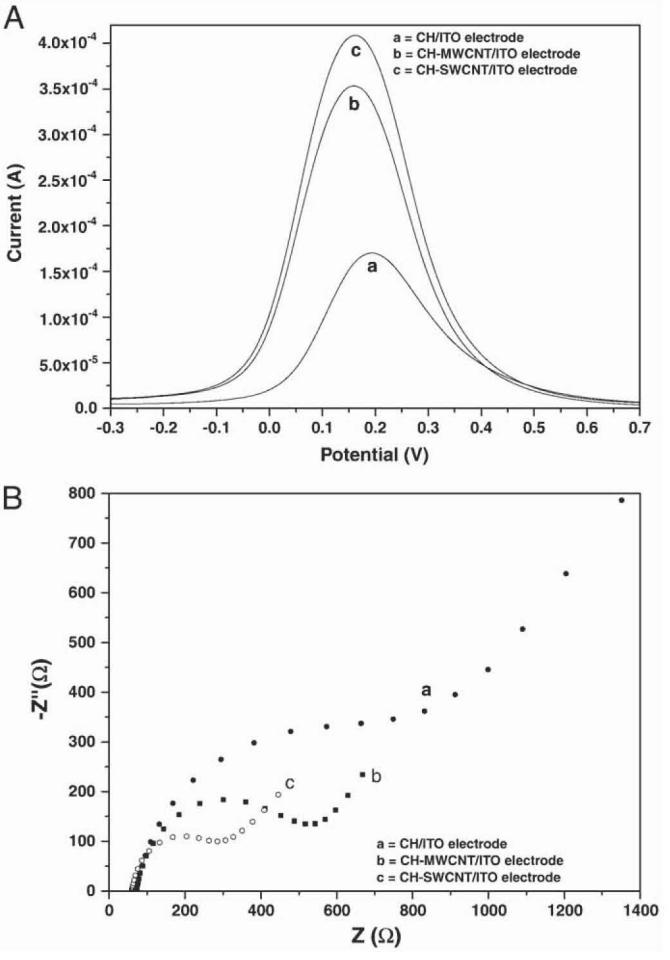

Fig. 2. A) DPV studies of CH/ITO (curve a), CH–MWCNT/ITO nanobiocomposite (curve b) and CH–SWCNT/ITO nanobiocomposite electrodes (curve c). B) EIS studies of CH/ITO (curve a), CH–MWCNT/ITO nanobiocomposite (curve b) and CH–SWCNT/ITO nanobiocomposite electrodes (curve c).

CH/ITO electrode (curve a), the semicircle located near the origin is probed by higher frequencies, which means that dynamics of the electron transfer in higher frequency range is observed and the current due to voltage excitation is under kinetic control. The low frequency region, where the slope of Z_{real} vs Z_{im} is dominated by mass transfer of the redox species and from the interfacial region. However, diameter of the semicircle for both the CH–MWCNT/ITO (curve b) and CH–SWCNT/ITO (curve c) nanobiocomposite electrodes decreases in comparison to that of the CH/ITO electrode revealing the incorporation of electrical conducting CNT embedded in the CH matrix increases the electro-active surface area of CH resulting in enhanced electron transport. The value of the charge transfer resistance (R_{CT}) for SWCNT/CH/ITO electrode is lower than that of the MWCNT/CH/ITO and this may be attributed to the open frame network and high electro catalytic properties of SWCNT that help in the easier electron transport. Hence, it is clear that the CH–SWCNT/ITO nanobiocomposite electrode exhibits good electrochemical behaviour than that of both the CH–MWCNT/ITO nanobiocomposite and CH/ITO electrode and may be suitable for electrochemical biosensor due to its perfect smaller electron transfer resistance.

Fig. 3B shows the DPV studies of stepwise formation of BSA/r-IgGs/CH–SWCNT/ITO (Fig. 3A) and BSA/r-IgGs/CH–MWCNT/ITO nanobiocomposite immunoelectrodes. The magnitude of the electrochemical response current further increases after the immobilization of r-IgGs onto the CH–CNT/ITO nanobiocomposite (curve c, Fig. 3A & B) revealing that CH–CNT provides a good environment for IgGs immobilization and available non-binding sites on r-IgGs making r-IgGs/CH–CNT/ITO immunoelectrode positively charged resulting in both increased diffusion of electrons and electron transport between r-IgGs and electrode. However, after the immobilization of BSA onto the r-IgGs/CH–CNT/ITO immunoelectrode (curve d, Fig. 3A & B) the magnitude of the current decreases due to blocking of the non-binding sites of r-IgGs/CH–CNT/ITO immunoelectrode resulting in hindered electron transfer between the medium and electrode confirming the immobilization of BSA onto r-IgGs/CH–CNT/ITO immunoelectrode. The similar results have been obtained in the CV studies (data not shown) of CH/ITO electrode, CH–SW/MW CNT/ITO nanobiocomposite electrode, r-IgGs/CH–SW/MW–CNT/ITO immunoelectrode and BSA/r-IgGs/CH–SW/MWCNT/ITO immunoelectrode). Interestingly, the magnitude of the current response of BSA/r-IgGs/CH–SWCNT/ITO immunoelectrode is higher than that of the BSA/r-IgGs/CH–MWCNT/ITO immunoelectrode, due to the three-dimensional arrangement and electro catalytic properties of SWCNT in the CH matrix to increase the electro-active surface area of CH–SWCNT nanobiocomposite for high loading of r-IgGs resulting in improved electrochemical properties of BSA/r-IgGs/CH–SWCNT/ITO immunoelectrode.

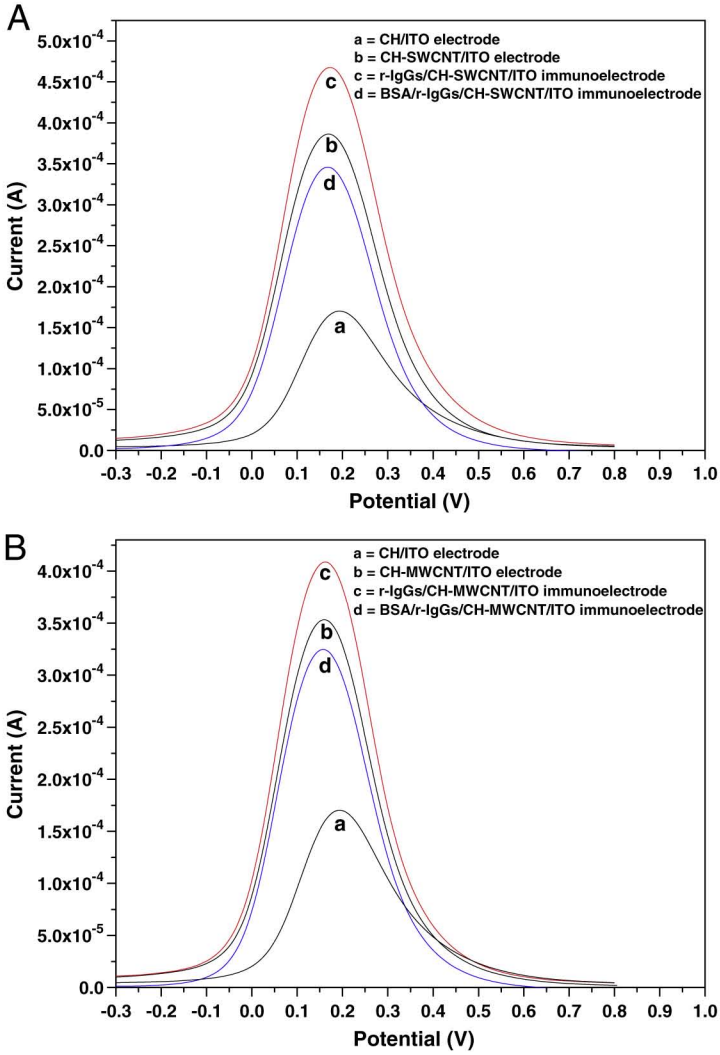

Fig. 3. A) DPV studies of CH/ITO (curve a), CH–SWCNT/ITO nanobiocomposite (curve b), r-IgGs/CH–SWCNT/ITO nanobiocomposite immunoelectrode (curve c) and BSA/r-IgGs/CH–SWCNT/ITO nanobiocomposite immunoelectrode (curve d). B) DPV studies CH/ITO (curve a), CH–MWCNT/ITO nanobiocomposite (curve b), r-IgGs/CH–MWCNT/ITO nanobiocomposite immunoelectrode (curve c) and BSA/r-IgGs/CH–MWCNT/ITO nanobiocomposite immunoelectrode (curve d).

The surface concentrations of ionic redox species on the CH/ITO electrode and CH–SWCNT/ITO nanobiocomposite electrodes, CH–MWCNT/ITO nanobiocomposite electrode have been estimated using Eq. (1) [40].

$$i_p = 0.227nFAC_o^* k^0 \exp\left[\frac{-\alpha n_a F}{RT}\left(E_p - E_0^{'}\right)\right] \quad (1)$$

where, i_p is the anodic peak current, n is the number of electrons transferred (1), F is the Faraday constant (96485.34 $C\,mol^{-1}$), A is surface area (0.25 cm^{-2}), R is the gas constant (8.314 $J\,mol^{-1}K^{-1}$), C_0^* is the surface concentration of the ionic species of film surface (mol cm^{-3}), E_p is the peak potential and E_0' is the formal potential. $-\alpha n_a F/RT$ and k^0 (rate constant) correspond to the slope and intercept of ln (i_p) vs the $E_p - E_0'$ curve at different scan rates. It may be noted that surface concentration of CH–SWCNT/ITO nanobiocomposite electrode (3.2×10^{-6} mol cm^{-3}), and CH–MWCNT/ITO nanobiocomposite electrode (2.4×10^{-6} mol cm^{-3}) are higher than that of the CH/ITO (1.4×10^{-6} mol cm^{-3}). The increased surface concentration of redox species onto the CH–CNT/ITO nanobiocomposite electrode reveals increased redox moieties that are available for oxidation leading to a higher faradic current wherein, the presence of CNT results in increased electron transport between redox species and electrode.

Fig. 4A and B show result of CV studies carried out on both BSA/r-IgGs/ CH–SWCNT/ITO (Fig. 3A) and BSA/r-IgGs/CH–MWCNT/ITO (3B) nanobiocomposite immunoelectrodes as a function of scan rate (10–100 mV/s). It can be seen that potential and magnitude of the response currents are dependent on the scan rate that exhibits a linear relationship with the sweep rate (*inset*: Fig. 3A and B) revealing that the electrochemical reaction is a diffusion-controlled process and facile electron transfer between medium and electrode [35].

The effect of pH on both BSA/r-IgGs/CH–SWCNT/ITO and BSA/r-IgGs/CH–MWCNT/ITO immunoelectrodes has been carried out using DPV technique (data not shown). It is observed that the magnitude of the current increases in the pH range from 6.0 to 7.0. The magnitude of the current has been found to decrease by further increasing the pH from 7.0 to 8.0. This suggests that both electrode show maximum activity at pH 7 at which r-IgGs and BSA retain their natural structure and do not denature. Thus all the experiments have been conducted at pH 7.0. The DPV analysis of CH/ITO electrode, CH–CNT/ITO nanobiocomposite electrode and BSA/r-IgGs/CH–SW/MW CNT/ITO immunoelectrodes have been repeated several times (~20 times) on the same film surface

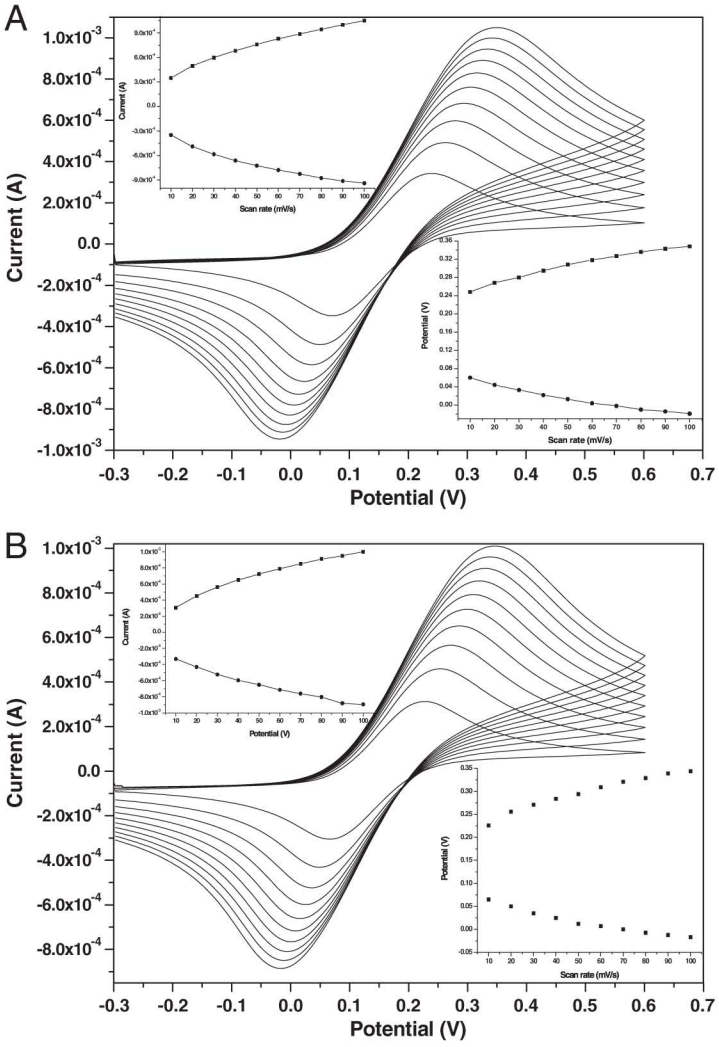

Fig. 4. A) CV studies of BSA/r-IgGs/CH–SWCNT/ITO nanobiocomposite immunoelectrode as function of scan rate (10–100 mV/s). B) CV studies of BSA/r-IgGs/CH–MWCNT/ITO nanobiocomposite immunoelectrode as function of scan rate (10–100 mV/s).

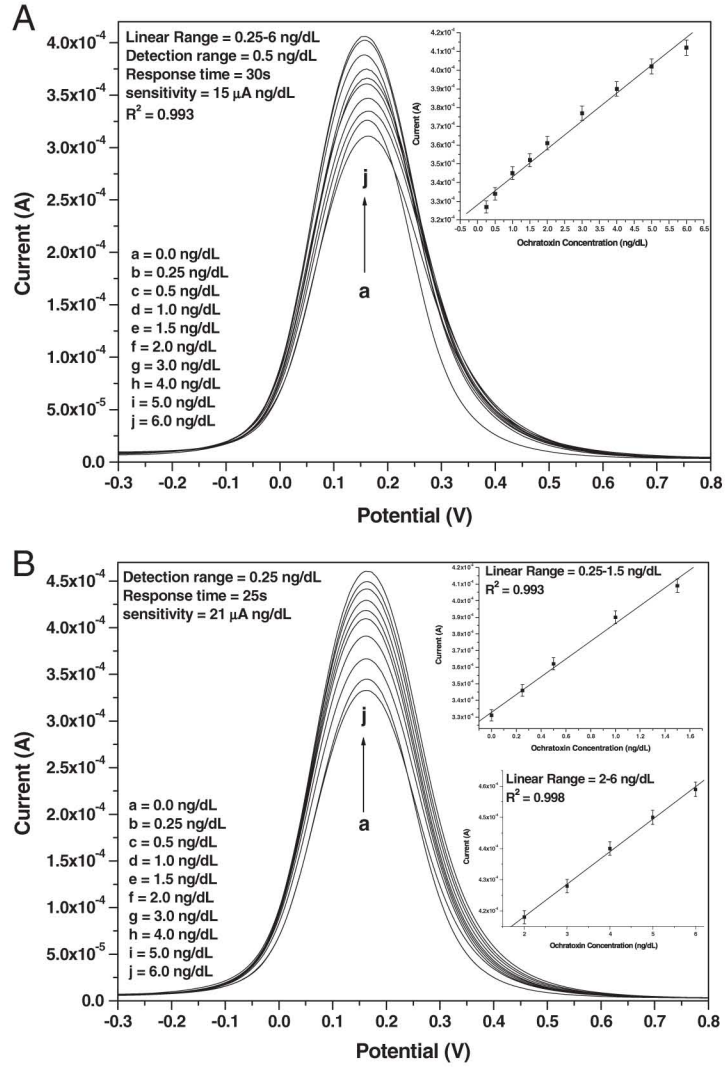

Fig. 5. Electrochemical response studies both BSA/r-IgGs/CH–MWCNT/ITO (A) and BSA/r-IgGs/CH–SWCNT/ITO nanobiocomposite immunoelectrodes (B) as function of OTA concentration (0.25–6 ng/dL).

in electrolyte and different films have been prepared from the same stock solution and the results are reproducible (with 4% error).

5. Electrochemical response studies

The electrochemical response of both the BSA/r-IgGs/CH–MWCNT/ITO (Fig. 5A) and BSA/r-IgGs/CH–SWCNT/ITO (Fig. 5**A**) immunoelectrodes has been investigated as a function of OTA concentration using DPV technique in PBS solution {50 mM PBS (pH 7, 0.9% NaCl) containing 5 mM $[Fe(CN)_6]^{3-/4-}$}. The magnitude of the electrochemical current response is found to be increase on the addition of OTA (0.25–6 ng/dL).

This can be attributed to the formation of antigen–antibody complex between OTA and r-IgGs on electrode surface that acts as electron transfer-accelerating layer resulting in the enhanced electron transfer between r-IgGs and electrode via CH–CNT nanobiocomposite. Inset in Fig. 5A shows the calibration curve of BSA/r-IgGs/CH–MWCNT/ITO immunoelectrode obtained as a function of OTA concentration. A linear relationship between the magnitude of current and OTA concentration can be fitted to the experimental points from 0.5 to 6 ng dL^{-1} and follows Eq. (2).

$$I(A) = 3.18 \times 10^{-4}(A) + 15\,\mu A\,dL\,ng^{-1} \times \left[OTA\ \ concentration\left(ng\,dL^{-1}\right)\right] \quad (2)$$

BSA/r-IgGs/CH–MWCNT/ITO immunosensor exhibits sensing characteristics such as low detection limit (0.25 ng dL^{-1}), reproducibility (15 times), long term stability (80 days) and sensitivity (15 μA/ng $dL^{-1}cm^2$) with the correlation coefficient as 0.993. The electrochemical response of BSA/r-IgGs/CH–SWCNT/ITO immunosensor (Fig. 5B) is also measured as a function of OTA concentration (0.25–6 ng/dL^{-1}) with improved sensitivity calculated from the slope of curve has been found to be 21 μA/ng $dL^{-1}cm^2$. It has been shown that good linearity is found in the low concentration range (0.25–1.5 ng dL^{-1}) and the current follows Eq. (3) with correlation coefficient of 0.995.

$$I(A) = 3.3 \times 10^{-4}(A) + 53.5 \times \mu A\,dL\,ng^{-1} \times \left[\text{OTA concentration}\left(ng\,dL^{-1}\right)\right] \text{with } R^2 = 0.995 \quad (3)$$

As OTA concentration increases from 2 to 6 ng dL^{-1}, the observed response current starts to level off due to the restriction of the r-IgGs–OTA reaction that changes the order of reaction. Interestingly, in the OTA concentration range (2–6 ng dL^{-1}) the change in the electrochemical response current follows Eq. (4).

$$I(A) = 3.97 \times 10^{-4}(A) + 10.5 \times \mu A\,dL\,ng^{-1} \times \left[\text{OTA concentration}\left(ng\,dL^{-1}\right)\right] \text{with } R^2 = 0.998 \quad (4)$$

However, due to the open frame network morphology and high electrocatalytic properties of SWCNT than that of the MWCNT, BSA/r-IgGs/CH–SWCNT/ITO immunosensor shows improved sensing

characteristics. The reproducibility of response of the immunoelectrode has been investigated at 1 ng dL^{-1} OTA concentration with the time interval of 7 days. No significant decrease in the current is observed revealing that immunosensor can be used ~15 times with a response time of 25 s and a shelf life ~90 days (data not shown). The apparent value of the association constant (*K*a) obtained as 4×10^{12} $Lmol^{-1}$ using a Lineweaver–Burke-like plot indicates high affinity of r-IgGs towards OTA due to prevalent electrostatic interactions. The high affinity of the BSA/r-IgGs/CH–SWCNT/ITO immunoelectrode can be attributed to favourable conformation of r-IgGs and increased loading of r-IgGs provided by the microenvironment of the CH and functionalized CNT nanobiocomposite platform [41].

6. Conclusions

In summary, r-IgGs and BSA have been co-immobilized onto CH–SWCNT/ITO and CH–MWCNT/ITO nanobiocomposite electrodes for OTA detection. Due to the open frame network and high electrochemical properties of SWCNT, BSA/r-IgGs/CH–SWCNT/ITO immunoelectrode exhibits better improvement than that of the CH–MWCNT nanobiocomposite immunoelectrode. BSA/r-IgGs/CH–SWCNT/ITO immunosensor may find potential application for the detection of other clinically important antigens such as aflatoxin, ochratoxin B, citrinin, ergot alkaloids, fumonisins, patulin, trichothecenes, and zearalenone etc.

Acknowledgements

We thank to Porf. R. C. Budhani, Director, National Physical Laboratory, New Delhi, India for providing facilities. A K and PRS are thankful to Department of Science and Technology (DST), India for the award of Senior Research Associate ship and Senior Research Fellowship.

References

[1] S. Iijima, Nature 354 (1991) 56.
[2] M. Ajayan, Chem. Rev. 99 (1999) 1787.
[3] J. Wang, Electroanalysis 17 (2007) 7.
[4] M.D. Rubianes, G.A., Electroanalysis 17 (2005) 73.
[5] M. Trojanowicz, Trends Anal. Chem. 25 (2006) 480.
[6] A. Merkoci, M. Pumera, X. Llopis, B. Perez, M.D. Valle, S. Alegret, Trends Anal. Chem. 24 (2005) 826.
[7] S. Sotiropoulou, N.A. Chaniotakis, Anal. Bioanal. Chem. 375 (2003) 103.
[8] S. Roy, H. Vedala, W. Choi, Nanotechnology 17 (2006) S14.
[9] Y. Yao, K.K. Shiu, Anal. Bioanal. Chem. 387 (2007) 303.
[10] M. Gao, L. Dai, G.G. Wallace, Electroanalysis 15 (2003) 1089.
[11] M. O'Connor, S.N. Kim, A.J. Killard, R.J. Forster, M.R. Smyth, F. Papadimitrakopoulosb, J.F. Rusling, Analyst 129 (2004) 1176.
[12] C. Dhand, S.K. Arya, M. Datta, B.D. Malhotra, Anal. Biochem. 383 (2008) 194.
[13] C. Dhand, S.K. Arya, S.P. Singh, B.P. Singh, M. Datta, B.D. Malhotraa, Carbon 46 (2008) 1727.
[14] P.J. Britto, K.S.V. Santhanam, P.M. Ajayan, Bioelectrochem. Bioenerg. 41 (1996) 121.
[15] M. Musameh, J. Wang, A. Merkoci, Y. Lin, Electrochem. Commun. 4 (2002) 743.
[16] J. Wang, M. Li, Z. Shi, N. Li, Z. Gu, Electroanalysis 14 (2002) 225.
[17] J. Wang, M. Li, Z. Shi, N. Li, Z. Gu, Anal. Chem. 74 (2002) 1993.
[18] Z. Wang, J. Liu, Q. Liang, Y. Wang, G. Luo, Analyst 127 (2002) 653.
[19] J. Wng, M. Li, Z. Shi, N. Li, Z. Gu, Electrochimica Acta 47 (2001) 651.
[20] R. Antiochia, I. Lvagnini, P. Pastore, F. Magno, Bioelectrochemistry 64 (2004) 157.
[21] N.S. Lawrence, R.D. Deo, J. Wang, Talanta 63 (2004) 443.
[22] J. Wang, A.N. Kawdw, M. Musameh, Analyst 129 (2003) 125.
[23] G.M. Spinks, S.R. Shin, G.G. Wallace, P.G. Whitten, S.I. Kim, S.J. Kim, Sensors Actuators B 115 (2006) 678.
[24] Y. Liu, J. Tang, X. Chen, J.H. Xin, Carbon 43 (2005) 3178.
[25] X.L. Luo, J.J. Xu, J.L. Wang, H.Y. Chen, Chem. Commun. (2005) 2169.
[26] M. Zhang, W. Gorski, J. Am. Chem. Soc. 127 (2005) 2058.
[27] X. Wei, J. Cruz, W. Gorski, Anal. Chem. 74 (2002) 5039.
[28] M. Zhang, A. Smith, W. Gorski, Anal. Chem. 76 (2004) 5045.
[29] J. Li, Qian Liu, Yingju Liu, Shanchao Liu, Shouzhuo Yao, Anal. Biochem 346 (2005) 107.
[30] Y. Liu, M. Wang, Feng Zhao, Zhiai Xu, Shaojun Dong, Biosens. Bioelectron 21 (2005) 984.
[31] X. Cui, C.M. Li, J. Zang, S. Yu, Biosens. Bioelectron. 22 (2007) 3288.
[32] Y. Wang, W. Wei, J. Zeng, X. Liu, X. Zeng, Microchim. Acta 160 (2008) 253.
[33] P.R. Solanki, A. Kaushik, A.A. Ansari, A. Tiwari, B.D. Malhotra, Sens. Actuators B 137 (2009) 727.
[34] J. Lin, C. He, L. Zhang, S. Zhang, Anal. Biochem. 384 (2009) 30.
[35] A. Kaushik, P.R. Solanki, A.A. Ansaril, S. Ahmad, B.D. Malhotra, Nanotechnology 20 (2009) 055105.
[36] A. Kaushik, P.R. Solanki, A.A. Ansari, S. Ahmad, B.D. Malhotra, Electrochem. Commun. 10 (2008) 1364.
[37] R.B. Mathur, S. Seth, C. Lal, R. Rao, B.P. Singh, T.L. Dhami, A.M. Rao, Carbon 45 (2007) 132.
[38] R.B. Mathur, S. Chatterjee, B.P. Singh, Compos. Sci. Technol. 68 (2008) 1608.
[39] K. Kan, T. Xia, L. Li, H. Bi, H. Fu, K. Shi, Nanotechnology 20 (2009) 185502.
[40] A. Kaushik, R. Khan, P. Pandey, J. Alam, S. Ahmad, B.D. Malhotra, Biosens. Bioelectron. 24 (2008) 676.
[41] J. Kuby, in: Richard A. Goldsby, Thomas J. Kindt, Barbara A. Osborne (Eds.), Kuby Immunology 4e, 4th ed., W. H. Freeman & Company, January 15 2000.